U.S. Department of Commerce
National Oceanic and Atmospheric Administration
National Weather Service
National Centers for Environmental Prediction
5830 University Research Court
College Park, MD 20740-3818

**Office Note 489**
http://doi.org/10.7289/V5/ON-NCEP-489

# SETS OF OPTIMALLY DIVERSIFIED POLYHEDRAL ORIENTATIONS

R. James Purser*
IM Systems Group, Rockville, Maryland

September 20, 2017



* email: jim.purser@noaa.gov

**Abstract**

Efficient integration of global atmospheric models on massively parallel computers is driving the move towards the use of discretizations based on regular polyhedra, such as the cube or icosahedron, and away from the traditional grids based on latitude and longitude alignments. In the case of NCEP's new proposed operational global model, the FV3, it is the equiangular modification of the gnomonic cubed-sphere grid that is being adopted. One risk of using any polyhedral grid is that the polyhedral shape itself will leave a subtle unwanted 'imprint' detectable in the long-duration accumulation of diagnostics from medium-range forecasts or from extended climate runs. Another difficulty relates to the numerical complications that arise from the interaction of a moving nested grid with the edges and corners of a cubic grid. These potential problems can presumably be mitigated if it is possible to switch among a prepared set of diversified grid orientations (provided the implied interpolations are performed in a sufficiently careful way that prevents them from inadvertently contributing to the imprinting problem).

In the case of extended integrations, the periodic interruption of the run in order to interpolate to the 'next' in a cycle of alternative grid orientations should help to prevent the imprinting of any single pattern of the polyhedron from becoming established. In the case of the tracking of a *single* compact feature, such as a tropical cyclone, using a dedicated nested grid within the polyhedral parent, the driving global grid can be switched periodically to whichever of the prepared set best maintains a respectful distance between its edges (and corners) and the compact feature, thereby eliminating the awkward interaction that occurs when a nest crosses the edge of the parent.

A further reason for wishing to possess a variety of cubic orientations is to provide the ability to 'randomize' the geometrical disposition of small sets of space-filling 'Hilbert curves' that can be used to facilitate grid-independent rough estimates of the local spatial density of the kinds of data (such as aircraft winds and temperatures) that exhibit a pronounced degree of clumpiness (whereas grid-based density estimates would become prohibitively costly).

This study analyzes the geometric characteristics of a nonredundant 'fundamental region' of the quaternionic rotation representation for each type of symmetry that a polyhedral global grid is likely to possess, such that any orientation whatsoever of the grid can be uniquely identified with a quaternion within this region. Then it is shown how finite sets of quaternions within each of these characteristic fundamental regions can be constructed to sample the space of inequivalent orientations of that grid in a systematic and representative way.

## 1. Introduction

In order to integrate a global atmospheric model at state-of-the-art resolutions in a reasonable time, it is necessary to use a massively-parallel computational architecture, and in order to then reduce the amount of inter-processor communications incurred, it appears to be necessary to abandon the spectral approach, as well as the traditional geographical grids based on latitude and longitude, and adopt grid-based numerical techniques whose grids are more amenable to efficient parallelization. Among such grids are the rectangular grids based on cubed-sphere geometries, such as is used by NCEP's next-generation FV3 global model (Lin and Rood 1997, Putman and Lin 2007) with a grid of the type schematically sketched in Fig. 1, or the triangular/hexagonal grids based on the icosahedral geometry (e.g., Bleck et al. 2015). An unfortunate and persistent problem associated with the adoption of polyhedral grids is that this type of geometry tends to become 'imprinted' as an unwanted artifact upon the long-term accumulated diagnostics of extended integrations, either in medium-range forecasts or in climate runs. Other difficulties caused by the adoption of a dedicated global polyhedral-grid parent model driving a finer-resolution mobile nested grid tracking a compact feature of interest, such as a tropical cyclone, are the severe numerical complications of the interaction of the nest when it is required to overlap with the edges or corners of the parent grid. These difficulties can presumably be mitigated or eliminated by judiciously switching among diverse prepared orientations of the global polyhedral grid. In the case of extended forecasts or climate integrations, a periodic and cyclic progression through a set of optimally diverse orientations (say, once per day of integration) should prevent any one cube or icosahedron's shape from having sufficient time to imprint itself strongly upon the solution (provided the transitional interpolations are carried out carefully to prevent these procedures themselves from imparting their unwanted imprint, of course).

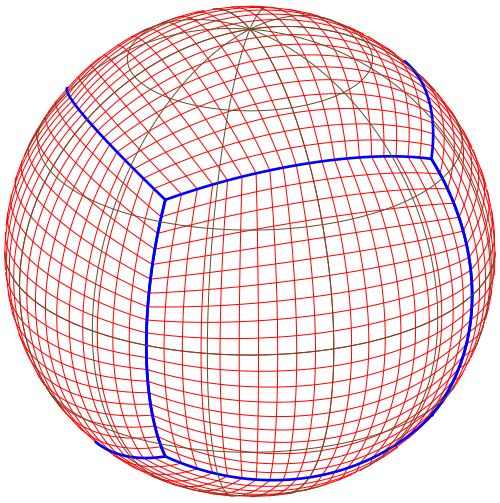

Figure 1. The equiangular gnomonic cubed sphere.

In the case of a dedicated global parent grid driving a daughter nest tracking a mobile

compact system, the periodic switch to a new orientation can be made judiciously to ensure that, for a period at least, the feature of interest remains far from edges and corners of the parent grid.

A further motivation for considering the construction of sets of diverse orientations of the cube relates to the completely different problem we face of estimating the spatial density of data types such as aircraft winds and temperatures where the data tends to clump in ways that would make the use of a fine grid-based estimation of data density prohibitively expensive; in this kind of situation, it is expected to be cheaper to project the data locations onto space-filling 'Hilbert curves' which are most easily constructed within a cubic framework (Purser et al., 2009), and to use the data density along the 'curve' as a rough surrogate for the spatial density. In order to make this trick viable and robust, it is probably necessary to average the estimates obtained with several 'randomized' orientations of the underlying cubic framework; in which case, we should aim to possess a small but maximally diverse set of orientations of the cubic framework within which the Hilbert curve is constructed.

While our primary focus will be on the geometry of rotations of the cube, the icosahedral case is also relevant to the cubic example since one of the best ways of raising the degree of symmetry of a set of cubes is to arrange them symmetrically around the regular icosahedron or its dual, the dodecahedron. We shall begin, in the next section, by reviewing the geometry of solid body rotations in terms of unit quaternions (also isomorphically equivalent to the Pauli spin matrices of spin-one-half particles in quantum mechanics), antipodal pairs of which most naturally describe the metric geometry intrinsic to spatial rotations. The inequivalent orientations of the cube and of the icosahedron have their own much reduced quotient spaces that we can identify with polyhedral subsets of the unit quaternions, induced by the respective symmetry groups, the octahedral group and the icosahedron group.

In section 3 we explore the relative merits of various special small sets of cubic rotations suggested by this geometrical picture. For mitigating grid-imprinting, it is desirable that the chosen set consists of elements that are as mutually diverse as possible and are at the same time (if possible) equivalent to one another by some symmetry in the domain of this space of rotations. It is also desirable (though not necessary) to be able to find a systematic cyclic tour through the set of orientations that maintains as large a 'distance' as possible between consecutive elements. In the context of providing sets of parent grids for a compact nest, the important criterion is the maximum radius we can associate with a given set of inscribed cubes such that, regardless of the geographical location of the nest center, we can guarantee that there is at least one member of our set whose cube-edges do not intersect a disk with this radius. For larger sets of orientations of the important griddable polyhedra, section 4 outlines some systematic approaches to producing quasi-uniform sampling of the fundamental regions representing the spaces of inequivalent rotations of these grid geometries to any degree of resolution. In this way, very large ensembles of each kind of grid can be generated that are approximately representative of all the possible orientations. Concluding discussions are presented in section 5.

## 2. Geometry of rotations and polyhedral symmetries

If we define the infinitesimal generators of three-dimensional (3D) rotations:

$$\boldsymbol{G}_x = \begin{bmatrix} 0 & 0 & 0 \\ 0 & 0 & -1 \\ 0 & 1 & 0 \end{bmatrix} \qquad \boldsymbol{G}_y = \begin{bmatrix} 0 & 0 & 1 \\ 0 & 0 & 0 \\ -1 & 0 & 0 \end{bmatrix} \qquad \boldsymbol{G}_z = \begin{bmatrix} 0 & -1 & 0 \\ 1 & 0 & 0 \\ 0 & 0 & 0 \end{bmatrix}, \tag{2.1}$$

we easily verify that $\boldsymbol{\alpha} = (\alpha_x, \alpha_y, \alpha_z)^T$ is a null eigenvector of the generator,

$$\boldsymbol{G} = \alpha_x \boldsymbol{G}_x + \alpha_y \boldsymbol{G}_y + \alpha_z \boldsymbol{G}_z, \tag{2.2}$$

and hence, it is an eigenvector with unit eigenvalue of the finite rotation matrix, $\boldsymbol{R}$, formed by constructing the *exponential map*, which just means applying the matrix exponential function:

$$\boldsymbol{R} = \exp\{\boldsymbol{G}\}. \tag{2.3}$$

This orthogonal matrix $\boldsymbol{R}$ represents a rotation by an angle, $\alpha = |\boldsymbol{\alpha}|$, in the right-handed sense about the axis pointing in the direction of $\boldsymbol{\alpha}$.

A *quaternion* (Conway and Smith 2003) can be defined as a real-valued four-vector $\boldsymbol{q}$ with component, $q_0$, conventionally denoted (confusingly) as the *real* (or *scalar*) component and the remaining three components, $q_1$, $q_2$, $q_3$, denoted the *imaginary* (or *vector*) components, with the usual additive property of vectors but also with a noncommutative multiplication rule such that, if $\boldsymbol{q}'' = \boldsymbol{q}'\boldsymbol{q}$, then the components of $\boldsymbol{q}''$ are defined

$$q''_0 = q'_0 q_0 - q'_1 q_1 - q'_2 q_2 - q'_3 q_3 \tag{2.4a}$$
$$q''_1 = q'_0 q_1 + q'_1 q_0 + q'_2 q_3 - q'_3 q_2 \tag{2.4b}$$
$$q''_2 = q'_0 q_2 - q'_1 q_3 + q'_2 q_0 + q'_3 q_1 \tag{2.4c}$$
$$q''_3 = q'_0 q_3 + q'_1 q_2 - q'_2 q_1 + q'_3 q_0. \tag{2.4d}$$

If we define the 'commutator' of a pair of quaternions using square brackets:

$$[\boldsymbol{q}_a, \boldsymbol{q}_b] = \boldsymbol{q}_a \boldsymbol{q}_b - \boldsymbol{q}_b \boldsymbol{q}_a, \tag{2.5}$$

we find that the real part of any commutator of quaternions vanishes and that, for any three quaternions, the Jacobi identity is satisfied:

$$[[\boldsymbol{q}_a, \boldsymbol{q}_b], \boldsymbol{q}_c] + [[\boldsymbol{q}_b, \boldsymbol{q}_c], \boldsymbol{q}_a] + [[\boldsymbol{q}_c, \boldsymbol{q}_a], \boldsymbol{q}_b] = 0. \tag{2.6}$$

If we define three quaternion generators by,

$$\boldsymbol{q}_x = (0, 1/2, 0, 0)^T \qquad \boldsymbol{q}_y = (0, 0, 1/2, 0)^T \qquad \boldsymbol{q}_z = (0, 0, 0, 1/2)^T, \tag{2.7}$$

then we find that commutators of pairs satisfy the *Lie algebra* (Gilmore 1974):

$$\Big[\boldsymbol{q}_x, \boldsymbol{q}_y\Big] = \boldsymbol{q}_z \tag{2.8a}$$
$$\Big[\boldsymbol{q}_y, \boldsymbol{q}_z\Big] = \boldsymbol{q}_x \tag{2.8b}$$
$$\Big[\boldsymbol{q}_z, \boldsymbol{q}_x\Big] = \boldsymbol{q}_y, \tag{2.8c}$$

identical to that obeyed by the respective matrix generators, $\boldsymbol{G}_x$, $\boldsymbol{G}_y$, $\boldsymbol{G}_z$ when 'commutator' is defined for matrices in the corresponding way:

$$[\boldsymbol{G}_a, \boldsymbol{G}_b] = \boldsymbol{G}_a\boldsymbol{G}_b - \boldsymbol{G}_b\boldsymbol{G}_a. \tag{2.9}$$

When we take the exponential function of purely imaginary (no real component) quaternions,

$$\boldsymbol{r} = \exp\{\boldsymbol{q}_x\alpha_x + \boldsymbol{q}_y\alpha_y + \boldsymbol{q}_z\alpha_z\}, \tag{2.10}$$

the satisfaction of the Jacobi identity, (2.6), guarantees that we generate elements of a Lie group (usually denoted $SU(2)$) in the same way that we generate the rotation group from operations of the type, (2.3). While the two groups are structurally similar locally (generators obeying the same Lie algebra) they are not the same globally; each element of the proper rotation or *Special Orthogonal* group, $SO(3)$, mapping to **two** antipodal elements of the unit-hypersphere of elements of the $SU(2)$ group of unit quaternions generated by $\boldsymbol{q}_x$, $\boldsymbol{q}_y$ and $\boldsymbol{q}_z$.

If we suppose a test body in its standard orientation has this orientation identified by the real unit quaternion, $(1, 0, 0, 0)^T$, and we apply a continuous rotation to it, angle $|\boldsymbol{\alpha}|$, about the axis defined by the unit vector, $(\alpha_x, \alpha_y, \alpha_z)/|\boldsymbol{\alpha}|$, the quaternion representation of this orientation rotates on the unit 3-sphere to:

$$\boldsymbol{q}_{\boldsymbol{\alpha}} = (\cos(|\boldsymbol{\alpha}|/2), \sin(|\boldsymbol{\alpha}|/2)\alpha_x/|\boldsymbol{\alpha}|, \sin(|\boldsymbol{\alpha}|/2)\alpha_y/|\boldsymbol{\alpha}|, \sin(|\boldsymbol{\alpha}|/2)\alpha_z/|\boldsymbol{\alpha}|)^T, \tag{2.11}$$

so that a 360° rotation causes the quaternion to migrate to its antipodal location; this illustrates why we need to identify each solid orientation with an *antipodal pair* of quaternions in order to avoid ambiguities.

If we take any given finite rotation, with quaternion represented by $\boldsymbol{q}_{\boldsymbol{\beta}}$, and observe the orbit of product quaternions when this is followed by $\boldsymbol{q}_{\boldsymbol{\alpha}}$ for angle $|\boldsymbol{\alpha}|$ cycling through a full 720°, we find that this orbit, $\boldsymbol{q}_{\boldsymbol{\alpha}}\boldsymbol{q}_{\boldsymbol{\beta}}$, maps out a great circle on the unit-3-sphere that twists once in a right-handed sense around the orbit of $\boldsymbol{q}_{\boldsymbol{\alpha}}$ itself, and maintains a constant angular distance from it. Conversely, if we observe the orbit formed when we reverse the order of operators, that is, $\boldsymbol{q}_{\boldsymbol{\beta}}\boldsymbol{q}_{\boldsymbol{\alpha}}$, then, as $|\boldsymbol{\alpha}|$ changes through 720°, the image of this product forms a left-handed relative twist once about the orbit of $\boldsymbol{q}_{\boldsymbol{\alpha}}$. The set of such twisted great circle orbits for *all* unit quaternions $\boldsymbol{q}_{\boldsymbol{\beta}}$ constitute what is called a *Hopf fibration* (e.g., Lyons, 2003) in both cases.

The valuable property of the quaternionic representation of finite rotations is that, being also a metric space in which the natural 'distance' between any two rotations is consistently defined to be proportional to the surface angular distance between the nearest two corresponding quaternions, we can very easily work out how close two rotations $\boldsymbol{\alpha}$ and $\boldsymbol{\beta}$ are to each other and quantify this measure by the angle $\gamma$, say, by which we need to further rotate the result of $\boldsymbol{\alpha}$ to achieve the orientation $\boldsymbol{\beta}$ where this third rotation is about some definite axis; this magnitude of $\gamma$ is then twice the angular distance between the corresponding unit quaternions, or simply:

$$\gamma = 2\arccos(\boldsymbol{q}_{\boldsymbol{\alpha}}\cdot\boldsymbol{q}_{\boldsymbol{\beta}}) = 4\arcsin(|\boldsymbol{q}_{\boldsymbol{\alpha}} - \boldsymbol{q}_{\boldsymbol{\beta}}|/2). \tag{2.12}$$

(The dot product, $\boldsymbol{q}_{\boldsymbol{\alpha}}\cdot\boldsymbol{q}_{\boldsymbol{\beta}}$ is also the scalar part of the quaternion product of $\boldsymbol{q}_{\boldsymbol{\alpha}}\boldsymbol{q}^*_{\boldsymbol{\beta}}$, where $\boldsymbol{q}^*$ denote the conjugate of $\boldsymbol{q}_{\boldsymbol{\beta}}$ obtained by switching the signs of its three the vector components.)

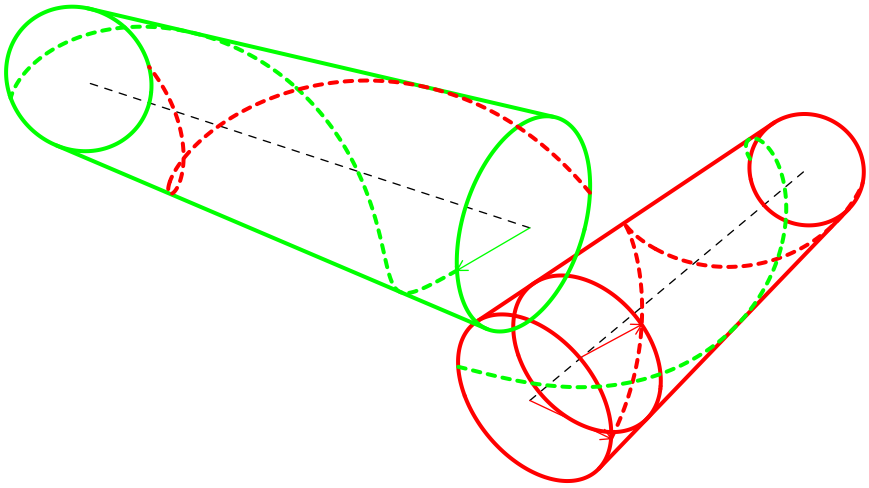

Figure 2. Two congruent mutually-entwined tori on the surface of the unit 3-sphere in the space of quaternions depicted here unwrapped, cut, and developed (with inevitable distortion) in Euclidean 3-space as a pair of touching cylinders. The set of inequivalent rotations of a spherical polar grid (like a conventional geographical lat-long grid) map to a region comprising only a single representative disk obtained as the section through one of these tori on the unit-quaternion 3-sphere (as well as the antipodal image of this disk, of course).

### (*a*) *Circular dihedron symmetry*

It is fair to assume that, owing to the effects of finite truncation errors aligned with the grid, any fine global grid used in a finite-difference or a finite-element discretization over the sphere will engender a macroscopic imprint on the solution reflecting the symmetry of the geometry of the grid. The latitude-longitude (lat-long) grid is a special example which, unlike any of the polyhedral grids we will consider, has an effectively continuous symmetry in one parameter, namely the longitude. The inequivalent orientations of the rotated lat-long grid on the fixed sphere can therefore be exhausted by the two-parameter set of locations within a fixed hemiphere of the pole of the grid that falls inside that hemisphere (or on one half of the equator in the special limiting case, to be strictly correct), with the further rotation of the grid about its own pole being immaterial. If we identify the orientation of the lat-long grid in its standard presentation (where its own pole coincides with the geographical north pole) with the real unit quaternion, $1 = (1, 0, 0, 0)^T$ (and its antipode, $-1$), then the direct rotation of the grid's pole to other locations in the geographical northern hemisphere, amounting to a total rotation of the frame by up to 90°, maps to a disk of angular radius 45° in the 3-sphere ('$S_3$') of unit quaternions, centered on $\boldsymbol{q} = 1$ and oriented perpendicular to the direction corresponding to that of the Earth's polar axis. Let us suppose that the Earth-centered Cartesian coordinates of a location with colatitude $\hat{\theta}$ and longitude $\lambda$ on the globe, in Earth-radius units, is:

$$(X, Y, Z) = (\sin\hat{\theta}\cos\lambda, \sin\hat{\theta}\sin\lambda, \cos\hat{\theta}). \tag{2.13}$$

In order to effect the rotation of the standard lat-long grid to place its pole at this location, the vector denoting this rotation must be,

$$\boldsymbol{\alpha}^T = (-\hat{\theta}\sin\lambda, \hat{\theta}\cos\lambda, 0). \tag{2.14}$$

and the corresponding quaternion, and its parameter bounds, are therefore,

$$\boldsymbol{q}_{\boldsymbol{\alpha}} = (\cos(\hat{\theta}/2), -\sin(\hat{\theta}/2)\sin\lambda, \sin(\hat{\theta}/2)\cos\lambda, 0)^T, \qquad \hat{\theta} \in [0, \pi/4], \quad \lambda \in [0, 2\pi). \tag{2.15}$$

This essentially defines a disk of the inequivalent representative orientations of a lat-long grid. Presumably, if an ensemble of forecasts were to be run using an ensemble of orientations spread over this disk with a density proportional to each element's degree of representation in the torus from which it is sliced, then the ensemble-averaged forecasts would be free of the imprinting that a fixed lat-long grid might otherwise impose.

If we 'turn' the lat-long grid a finite amount about its polar axis, and then further rotate its orientation as above, the effective total set of rotations thus generated would fill the torus on the surface of the quaternion unit-3-sphere comprising all points within an angle $\pi/4$ of the great circle,

$$\boldsymbol{q}_{\eta} = (\cos(\eta/2), 0, 0, \sin(\eta/2))^T, \tag{2.16}$$

where $\eta$ is the angle by which the grid is first spun about its polar axis. (Note that the antipodal pairs that correspond to the given rotated configuration occupy this *same* torus, not the complementary one.) The complement of this toroidal region is an exact copy, each torus wrapping around the other to fill the whole 3-sphere, and where the orientations described by the complementary torus comprise orientations of the grid once it has been 'flipped' enough to rotate its pole into some point in the opposite hemisphere. If we cut and 'develop' or unwrap the two tori as a pair of touching cylinders in three Euclidean dimensions, we have something resembling the arrangement shown in Fig. 2, which allows us to more easily see how one cyclinder/torus, by rolling over its complement, makes contact at each point in its own surface with some point on the surface of its complement. However, any development of a body on the surface of the 3-sphere flattened into the Euclidean 3-space involves some unavoidable distortion, which the picture does not help us to imagine.

Where we have sliced the red torus of Fig. 2 to form the end of the cylinder in this schematic development, we also show, by the red arrow, 45° in extent in quaternion $S_3$ space, pointing to the mutual surface of both tori, at a point that corresponds to a 90° rotation in physical space that would rotate the original coordinate polar axis to a point on the Earth's equator. But suppose we considere this rotation from the perspective of another polar grid system equivalent to the first except with a small shift in its datum of longitude. This rotated coordinate frame corresponds to a point on the axis of the (red) torus positioned slightly inward from the nearest end shown in the figure, and the 'fundamental region' of further rotations of this frame about axes in the equatorial plane correspond to the section of the torus at this inboard point. Then the exactly equivalent final orientation from the perspective of this new frame's fundamental region would correspond to the second red arrow shown in the plane of this slightly inward section of the torus. This second red arrow is twisted in the left-handed sense relative to the first, and the locus of all end points of such arrows, for *all* the possible spherical coordinate frames that have their polar axis in common, forms the Hopf fiber shown by the red dashed curve winding, in a left-handed helix, around the red torus (though it is actually a great-circle in the true quaternionic geometry that this developed picture distorts). The image of this same Hopf fiber on the boundary of the complementary green torus is also shown as a red dashed curve, and also winds around that torus in a left-handed sense. If we had chosen to rotate

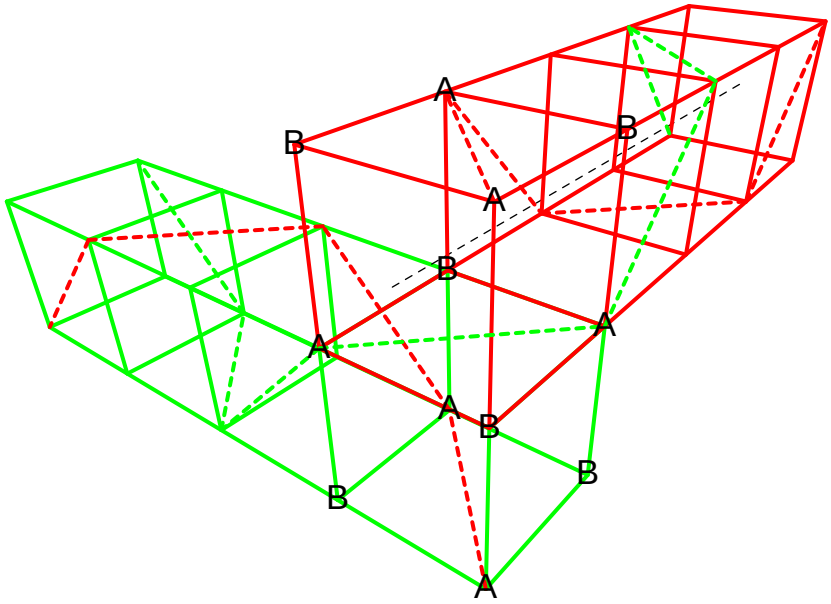


Figure 3. A tesseract or hypecube development into Euclidian 3-space arranged to show how it can be thought of approximately as two congruent mutually-entwined segmented tori, four cubes in a line forming each torus. However, as copies of the representative quaternionic region of inequivalent rotations (in Euclidean 3-space) of the rectangular dihedron, where the cells are projected onto the surface of the unit 3-sphere in the space of quaternions, we must think of each successive copy of the cubic regions as being twisted by a right-angle, and in the left-handed sense, as we follow each line of cells around the chain of any chosen torus.

the original polar coordinate frames by the same 90° angle but in the opposite sense, the Hopf fiber of equivalent orientations in the quaternionic representation would image to the green dashed curves (pointed to at one point by the green arrow). It is a characteristic of grids with symmetries that the equivalent orientations, relative to frames formed by rotating the grid into coincidence with itself, fall, usually as strings of discrete points, along such left-handed Hopf fibrations, as we shall see in the several examples of discrete grid symmetries treated below. This applies not only to the extreme rotations mapping to the fundamental region boundaries exemplified by the dashed curves in the figure, but equally to any of the 'interior' coordinate frame rotations by angles of smaller magnitudes.

(*b*) *Polygonal dihedral symmetries*

Another way to grid the surface of the globe is by using a spherical polygonal dihedron – defined as a degenerate two-sided polygonal polyhedron mapped over the sphere. As a simple (if impractical) illustrative example, a rectangular dihedral grid would map each hemisphere of the globe to a (nonsquare) rectangular grid, so that the group (an example of a representation of the abstract *Klein Four-Group*) of proper rotational symmetries is just the set of four derived by the identity, together with the 180° rotations about each one of the Cartesian $X$, $Y$, or $Z$ axes. The corresponding eight quaternions (four antipodal pairs) to which these equivalent grid-rotations belong are simply the vertices of the four-dimensional *cross-polytope* or *orthoplex*:

$$\pm\boldsymbol{q}_1 \quad = \quad \pm(1,0,0,0)^T \tag{2.17a}$$

$$\pm\boldsymbol{q}_x = \pm(0,1,0,0)^T \tag{2.17b}$$
$$\pm\boldsymbol{q}_y = \pm(0,0,1,0)^T \tag{2.17c}$$
$$\pm\boldsymbol{q}_z = \pm(0,0,0,1)^T, \tag{2.17d}$$

or, equivalently, the centers of the eight cells of the dual regular polytope, the *hypercube* or *tesseract* with edges of length two units. A general introduction and discussion of regular polytopes is to be found in Coxeter (1963); the '*twisted honeycombs*' of possibly less-regular polytopes that we shall be concerned with, and their quaternionic contexts, are described in Coxeter (1970), who notes that the group formed by the above eight quaternions is the classical *Quaternion Group*. The representative sets of inequivalent rotations of this grid can be identified with the '*Voronoi*' sets of these eight unit quaternions – that is, a projection onto the unit hypersphere of the cells of the hypercube or tesseract, where the given points are at the centers of the eight cubic cells. A Voronoi decomposition of a domain associated with a number of discrete points divides the region into cells of an equal number, each containing one of the points together with all those points closer to that point than to any other of the set. While the rectangular dihedron grid itself is probably of no practical interest as a framework for global modeling, this is probably the simplest possible example showing how the Voronoi construction can be employed to provide the tidiest set of inequivalent orientations of a grid configuration that possesses nontrivial rotational symmetries. The Voronoi cell that contains the identity quaternion provides a 'fundamental region' for the set of inequivalent rotations of the polyhedron under consideration. While, as we shall see, the connected fundamantal regions are not necessarily Voronoi in general, in this special example, the only consistent definition of the connected set of inequivalent rotations *is* Voronoi. A picture of one development into Euclidean 3-space of the eight-cube tesseract is shown in Fig. 3, where the arrangement is deliberately made to resemble, as nearly as possible, the double-toroidal depiction of Fig. 2 and the same Hopf fibers are shown, but now linking equivalent orientations 'A' at four discrete points along each fiber. The 16 vertices represent the most extreme rotations possible within each fundamental cubic region of the hypersphere, but by the symmetries induced in the quaternionic picture by the the four symmetries of the grid, only two types of vertices, 'A' and 'B' are inequivalent (i.e., there are eight copies of each type).

A slightly more practical example of a group of solid rotations that can be associated with spherical-polyhedral grids might be the square dihedral group. In addition to the obvious square-dihedron grid that the name suggests, this group describes the symmetries also of the alternating-sided octagonal dihedral grids proposed by Purser and Rančić (1997), or the square-prism modification of the cubed-sphere grid recently proposed by Purser and Tong (2017). Proper rotations comprise four rotations by multiples of right-angles about the (polar) $Z$-axis, together with 180° flips about the four symmetrical diameters. These eight rotations map to eight antipodal pairs of unit quaternions, forming the Voronoi centers of a pair of segmented octagonal-shaped approximate tori, shown in development in Fig. 4. Each fundamental representative region is a square-sided octagonal prism; that is, *any* obliquely rotated version of the grid this symmetry group describes can be identified by a unique point in the interior, or on one nonredundant half of the surface, of one chosen fundamental region of this set.

If we assume the axis of the standard dihedron is the usual $z$ axis, and denote $\rho = 1/\sqrt{2}$, then the cyclic subgroup of eight quaternions that form the Voronoi centers of one of the segmented

polyhedral-tori can be listed as the columns of the matrix:

$$\boldsymbol{Q}_1 = \left\{ \begin{array}{cccccccc} 1 & \rho & 0 & -\rho & -1 & -\rho & 0 & \rho \\ 0 & 0 & 0 & 0 & 0 & 0 & 0 & 0 \\ 0 & 0 & 0 & 0 & 0 & 0 & 0 & 0 \\ 0 & \rho & 1 & \rho & 0 & -\rho & -1 & -\rho \end{array} \right\}, \tag{2.18a}$$

while the other *coset* of this subgroup, forming the centers of the complementary polyhedral torus, are:

$$\boldsymbol{Q}_2 = \left\{ \begin{array}{cccccccc} 0 & 0 & 0 & 0 & 0 & 0 & 0 & 0 \\ 1 & \rho & 0 & -\rho & -1 & -\rho & 0 & \rho \\ 0 & \rho & 1 & \rho & 0 & -\rho & -1 & -\rho \\ 0 & 0 & 0 & 0 & 0 & 0 & 0 & 0 \end{array} \right\}. \tag{2.18b}$$

The rigid (metric-preserving) rotation and reflection symmetries, i.e., the discrete subgroup of the full orthogonal group, $O(4)$, acting in the space of the quaternions themselves, that keep invariant the set of these 16 column vectors of $\boldsymbol{Q}_1$ and $\boldsymbol{Q}_2$, forms what we shall refer to as an *isometry group* of 512 elements in this case (each quaternion and its neighborhood can be mapped to any of the 16, and with 32 orientations). The significance of this larger group of rigid permutations of the quaternionic *binary-group* or *bi-cyclic group* representation of the 3D polyhedral proper rotation group is that it helps us to characterize, in a more general way than the Voronoi construction, sufficient properties of any valid connected *fundamental region* of the $S_3$ associated with the quaternion configuration.

Replications of a valid fundamental region by the elements of the larger group must certainly cover $S_3$ without gaps or overlaps of finite measure; but they need not be Voronoi regions in the general case. This is because not all the boundary faces of the fundamental Voronoi region correspond to mirror-reflection planes of symmetry of the larger isometry group. In the present case, the binary group representation of symmetries of the square dihedron, the eight square sides of the octagonal prism defining the Voronoi cell do *not* lie within reflection planes of the isometry group (although the octagonal faces do). The diagonals of the square sides are axes of symmetries of 180° *gyrations* within the isometry group, and so these special lines, and the points that lie on them, *are* invariant, and must therefore lie on the boundary of *any* valid fundamental region; but we could choose to symmetrically corrugate the square face alternately inward and outward around the center of the square, keeping these diagonal axes fixed, and still have an acceptable definition of a connected fundamental region satifying the isometry group of symmetries. This subtlety will become relevant to how we propose to generate large representative ensembles of rotated dihedral grids in section 4. (In the previous example of rectangular-dihedron symmetries, the faces of the resulting tesseract projection onto the quaternionic $S_3$ *were* on mirror-reflection planes of the corresponding isometry group (of order 384) of the symmetries of the tesseract; the Voronoi definition was therefore the *only* valid way to define the fundamental region in that special case.)

More generally, the $2N$ proper rotational symmetries of a dihedron of any regular polygon of $N$ sides have Voronoi cells in the associated quaternionic $S_3$ representation of the binary group that each comprise the central projection onto this 3-sphere, from the tangent space orthogonal to its quaternion, of that one of the $4N$ congruent square-sided prisms of regular

$N$-gon cross-section. Again, these cells are organized into a pair of cyclic chains of $2N$ cells each, interlocking as (approximately) a pair of tori as before. The successive equivalent frames around each cycle are twisted relative to their predecessor in the chain by a left-handed angle of $\pi/N$. Again, in the general case, $N > 2$, while the Voronoi decomposition defines one valid fundamental region, it is not the only valid definition for exactly the same reason as before.

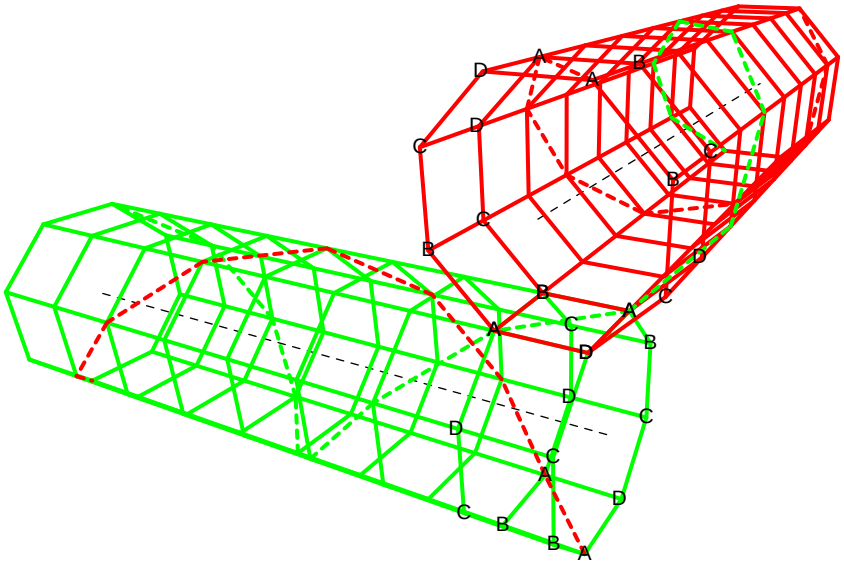


Figure 4. The sixteen Voronoi regions of the development into Euclidean 3-space of the binary group of square-dihedral symmetries represented by unit quaternions. Rotations about the normal axis of the dihedron by multiples of right-angles correspond to translations, with $\pi/8$ twists, along the cyclic chain of one of the approximate tori; the flip of the dihedron that exchanges its poles corresponds to movement and twist of $\pi/2$, in the quaternion space, between one of the eight points in the chain forming one torus, and a similar point of the alternative torus. Although each fundamental Voronoi region is a (curved) polyhedron embedded in the 3-sphere and possessing 16 vertices, these amount to only four inequivalent rotations, labelled A through D.

In the case of the square dihedron whose quaternionic developed segmented tori are depicted in Fig. 4, the extreme rotations of the grid still belong to the same fundamental region comprising four inequivalent vertex types, marked A–D in the figure. To see that the point 'A' is indeed equivalent in all four copies around the representative fundamental region, we exploit the fact that the rotational symmetries of the square dihedron are also a subset of the rotational symmetries of this octagonal prism. Thus, in Fig. 5 we can show the effect of rotating this octagonal prism about the four axes marked 'A' that result in the same effective final orientation of both the prism, together with the square dihedron, shown is blue, inscribed within it.

### (*c*) *Octahedral symmetries*

We next consider the double-cover of the rotation group (i.e., the binary group) of the cube represented in the quaternionic $S_3$. The proper rotations of the cube (usually denoted the *octahedral group* after the polyhedral dual of the cube) comprise 24 symmetries as follows: the identity; the six 90° rotations about the face-centers; the three 180° rotations about the face-centers; six 180° rotations about edge-midpoints; eight 120° rotations about vertex axes. So we expect to find the binary octahedral representation of the cube's rotation group comprising

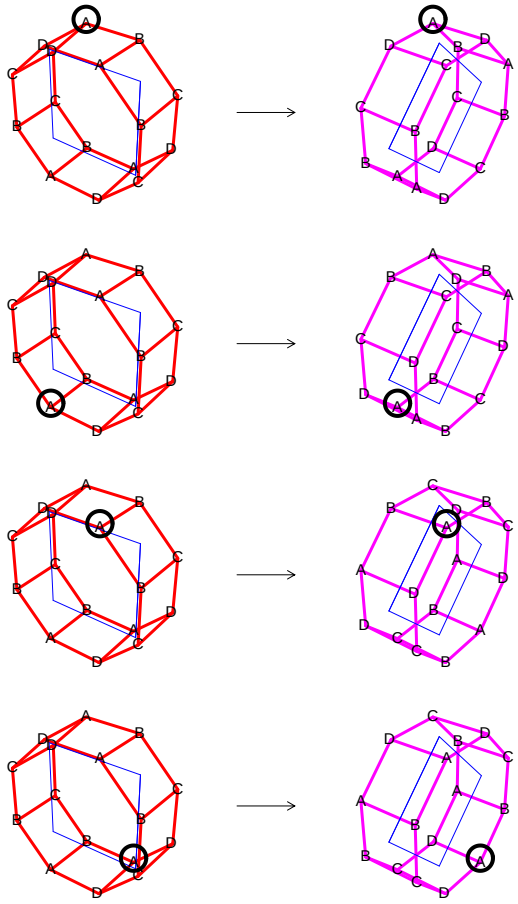

Figure 5. For the quaternionic representation of a fundamental region of the inequivalent rotations of a square-dihedral grid (or one of the other grids sharing the same symmetry) the 16 vertices of the square-sided octagonal prism are not independent, but rather form a set of only four distinct inequivalent rotations. We can illustrate this by rotating a copy, in ordinary 3-space, of the shape of the 'flat' projection of the fundamental region itself, and apply to it the rotations implied by the four rotation vectors formed by an origin at the body center and the four vertices marked 'A'. Inscribed within the shape is a depiction of an actual square dihedron which is rotated into the same rotated copy of itself by all four of the implied dicrete rotation vectors 'A'. In this context, we therefore treat each 'A' point as the *same* point in this restricted space of rotations. The same applies to the other vertex points marked 'B', 'C' and 'D', of course.

48 unit quaternions. 24 of these form a subgroup and are the vertices of the self-dual regular polytope, known as the *24 cell*; they are important in abstract algebra as defining the totality of *Hurwitz units* (Conway and Smith, 2003). Hurwitz integers are quaternions whose components are either all whole integers or all half-odd-integers. By themselves the Hurwitz units form the *binary tetrahedral group* corresponding to the 12 proper rotations of the regular tetrahedron that one can inscribe in the cube by linking vertices that share no edges. One normal subgroup of order eight, which we denote here by $\boldsymbol{H}_1$, is simply the double cover of the group of symmetries of a rectangular dihedron that we encountered earlier, i.e., the classical quaternion group itself.

The other two cosets of $\boldsymbol{H}_1$ within the tetrahedral group will be called $\boldsymbol{H}_2$ and $\boldsymbol{H}_3$. Thus,

$$\boldsymbol{H}_1 = \left\{ \begin{array}{cccccccc} 1 & -1 & 0 & 0 & 0 & 0 & 0 & 0 \\ 0 & 0 & 1 & -1 & 0 & 0 & 0 & 0 \\ 0 & 0 & 0 & 0 & 1 & -1 & 0 & 0 \\ 0 & 0 & 0 & 0 & 0 & 0 & 1 & -1 \end{array} \right\}, \tag{2.19a}$$

$$\boldsymbol{H}_2 = \frac{1}{2} \left\{ \begin{array}{cccccccc} 1 & -1 & 1 & -1 & 1 & -1 & 1 & -1 \\ 1 & -1 & 1 & -1 & -1 & 1 & -1 & 1 \\ 1 & -1 & -1 & 1 & 1 & -1 & -1 & 1 \\ 1 & -1 & -1 & 1 & -1 & 1 & 1 & -1 \end{array} \right\}, \tag{2.19b}$$

$$\boldsymbol{H}_3 = \frac{1}{2} \left\{ \begin{array}{cccccccc} 1 & -1 & 1 & -1 & 1 & -1 & -1 & 1 \\ 1 & -1 & 1 & -1 & -1 & 1 & 1 & -1 \\ 1 & -1 & -1 & 1 & 1 & -1 & 1 & -1 \\ -1 & 1 & 1 & -1 & 1 & -1 & 1 & -1 \end{array} \right\}. \tag{2.19c}$$

Geometrically, this decomposition reflects the property that the vertices can be partitioned amongst three distinct inscribed cross-polytopes. The remaining 24 elements completing the double-cover of the octahedral group (and forming the complementary coset of our binary tetrahedral group) are found as the unit-magnitude vertices of the polytope dual to our original 24-cell, another congruent 24-cell. The group $\boldsymbol{H}_1$ is also a normal subgroup of the full binary octahedral group, so left- and right-cosets coincide, suggesting that these additional vertices might also be organized into the additional unambiguous cosets of $\boldsymbol{H}_1$:

$$\boldsymbol{H}_4 = \left\{ \begin{array}{cccccccc} \rho & -\rho & \rho & -\rho & 0 & 0 & 0 & 0 \\ \rho & -\rho & -\rho & \rho & 0 & 0 & 0 & 0 \\ 0 & 0 & 0 & 0 & \rho & -\rho & \rho & -\rho \\ 0 & 0 & 0 & 0 & \rho & -\rho & -\rho & \rho \end{array} \right\}, \tag{2.19d}$$

$$\boldsymbol{H}_5 = \left\{ \begin{array}{cccccccc} \rho & -\rho & \rho & -\rho & 0 & 0 & 0 & 0 \\ 0 & 0 & 0 & 0 & \rho & -\rho & \rho & -\rho \\ \rho & -\rho & -\rho & \rho & 0 & 0 & 0 & 0 \\ 0 & 0 & 0 & 0 & \rho & -\rho & -\rho & \rho \end{array} \right\}, \tag{2.19e}$$

$$\boldsymbol{H}_6 = \left\{ \begin{array}{cccccccc} \rho & -\rho & \rho & -\rho & 0 & 0 & 0 & 0 \\ 0 & 0 & 0 & 0 & \rho & -\rho & \rho & -\rho \\ 0 & 0 & 0 & 0 & \rho & -\rho & -\rho & \rho \\ \rho & -\rho & -\rho & \rho & 0 & 0 & 0 & 0 \end{array} \right\}, \tag{2.19f}$$

where, again, $\rho = 1/\sqrt{2}$.

As in the case of the symmetries of dihedra, we find that the discrete orthogonal symmetries of O(4) that preserve this configuration of 48 quaternions (in this case, the order of the isometry group is 2304) greatly outnumber the elements of the binary octahedral group itself, and include many mirror-reflections and many 180° gyrations. The Voronoi cells are now the central projections onto the unit 3-sphere of the polyhedral cells of an irregular polytope whose polyhedra are truncated cubes – that is, six regular octagons and eight equilateral triangles,

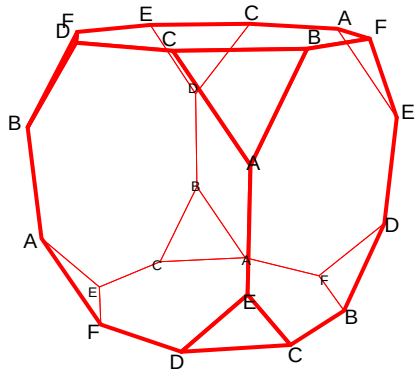


Figure 6. A representative fundamental Voronoi region containing corresponding to a set of inequivalent solid rotations of a cube.

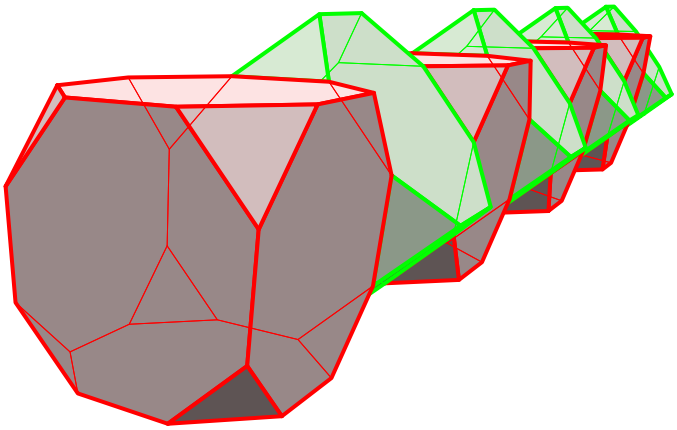

Figure 7. Eight fundamental Voronoi regions forming the central strand of a polyhedral segmented torus.

as shown in Fig. 6. But the octagonal faces do *not* lie within any mirror-planes – only the smaller triangular faces do. Thus, while a representative Voronoi cell serves as a possible, and geometrically convenient, fundamental region for all the inequivalent solid rotations of a cube, it is again not the *only* valid choice of a fundamental region. If we do adopt it, we note, as always with these decompositions, that half of the faces are redundant (each face being a slightly left-twisted copy of its opposite face). To see how the 'space' of the unit sphere is tiled by these shapes, a cyclic chain of eight of them, suitably twisted by $\pi/4$ at each step along the chain, is depicted in Fig. 7. To each one of these, we can attach a stradding pair of appropriately aligned neighbors forming an additional pair of twisted strands in the developed pattern shown in Fig. 8. This screw-torus can be shown to perfectly engage with an orthogonally entwined copy (Fig. 9) when this developed arrangement is folded up (in the four Euclidean quaternion dimensions) to close all the gaps.

Since each edge of the Voronoi cell is shared by three copies of the cell, there are only 12 such edges that are inequivalent (and therefore nonredundant). Similarly, since each vertex is

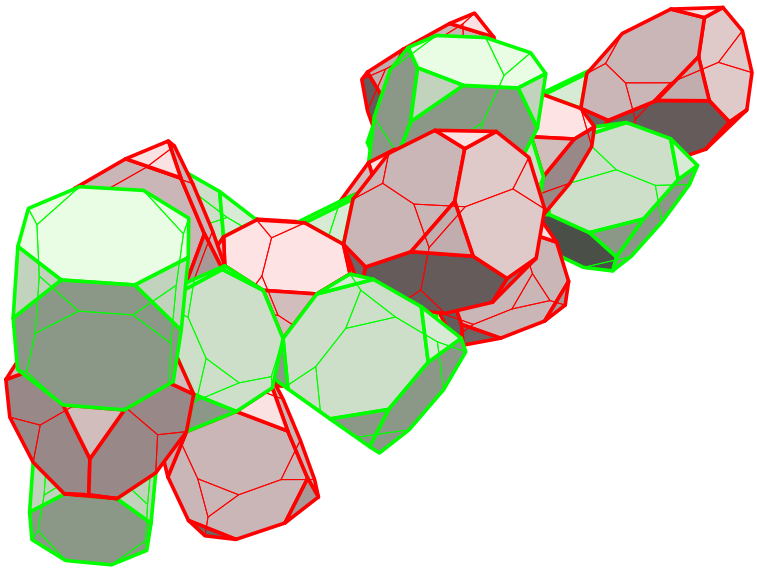

Figure 8. 24 fundamental Voronoi regions forming a polyhedral segmented screw-torus.

shared by four cells, there are only six vertices that are inequivalent. These are marked A–F in Fig. 6. If we wish to generate small ensembles of cubes with diversified orientations, we can preserve the overall cubic symmetry of the ensemble by picking nonredundant sets of the special points on the surface of the fundamental cell. For example, the centers of the Voronoi cell's faces provide three inequivalent mutually-rotated cubes for a symmetric ensemble of three. Although these faces are not themselves symmetry-invariants of the isometry group, their central points *are* since they lie at the intersection of (four) gyration axes. The 12 inequivalent edge midpoints of the Voronoi cell are *not* invariant points of the isometry group, being the intersections of only two mirror-planes in each case, whereas three nondegenerate planar intersections would be required to fix a point. For the same reason, the 12 edges themselves are also not invariants of the larger symmetry either. But the six inequivalent vertices of the Voronoi cell *are* invariant points of the isometry group by virtue of each being intersected by gyration axes. Thus, a symmetric ensemble of six rotated cubes is suggested by this set. We shall investigate the sets of rotated cube orientations suggested by these symmetry considerations in greater detail in section 3.

For a larger variety of diversified rotations of a cubic grid framework, we must also consider including rotations that correspond to points interior to the Voronoi cell. There is then an opportunity to do this in such a way that the ensemble as a whole possesses an even higher order of symmetry than that of the cube itself; that is, if we exploit a construction based on the higher icosahedral symmetry, a subgroup of which is the tetrahedral symmetry group which, as we have seen, amounts to one half of the symmetries of the cube. It is mainly for this reason that it is important to examine this icosahedral group in the context of quaternion representations, even when our object of interest is a cubic grid.

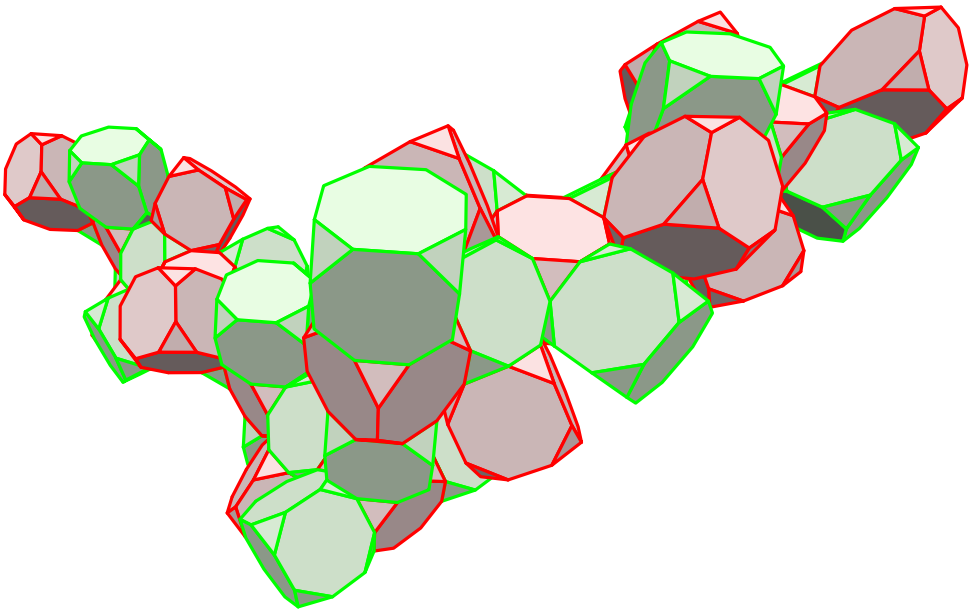

Figure 9. Two copies of the screw-torus shown in Fig. 8 wrap around each other when folded and projected onto the unit 3-sphere, closing all the gaps and partitioning the space of rotations into copies of the single fundamental Voronoi region in which all inequivalent rotations of a cubic grid can be mapped.

(*d*) *Icosahedral symmetries*

The proper solid rotations of a regular icosahedron, or its dual, the regular dodecahedron, form a group of order 60, and therefore a double-covering group, the *binary icoshedral group*, comprises the corresponding 120 unit quaternions, sometimes called the *icosians*. We shall find it more convenient to relate these symmetries to the dodecahedron (an example of which is shown in Fig. 10), since this is also precisely the shape of the cells of the polytope (the *120-cell*) whose central projection onto $S_3$ gives us the Voronoi regions describing the inequivalent rotations of an icosahedral grid. In this case, the connected fundamental region is necessarily this Voronoi cell since its faces all lie in mirror-reflection planes of the larger (order 14400) isometry subgroup of $O(4)$ by which this configuration of icosians can be rigidly transformed into itself.

The 60 proper rotations of the dodecahedron can be broken down as follows: the identity; 12 right-handed rotations of 72° about each of the face-centers; 12 right-handed rotations of 144° about these same axes; 15 rotations of 180° about axes through edge midpoints; 20 rotations of 120° about vertices. From these, the icosians can be shown to have a presentation that includes our 24-cell points, $\boldsymbol{H}_1 \cup \boldsymbol{H}_2 \cup \boldsymbol{H}_3$ together with the 96 points formed by all even permutations and sign combinations of the components:

$$q = [\phi, 1, 0, 1/\phi]^T \,, \tag{2.20}$$

where $\phi = (\sqrt{5}+1)/2$ defines the *Golden Number*.

The Voronoi regions of this set are the dodecahedral cells of the regular *120-cell* centrally projected into the 3-sphere. A single cell, Fig. 10, with vertices labeled A–E as shown, can be

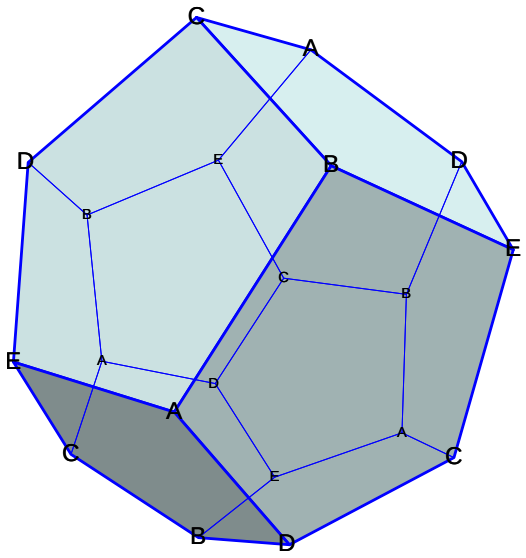


Figure 10. The regular dodecahedron labeled with five inequivalent vertices when used to define the dodecahedral space of rotations of the icosahedral symmetry.

joined to its replicates where each is translated and rotated to the left 36° each step along a given chain of ten that then joins itself to form a cycle. A *discrete* Hopf fibration of 12 such cycles entwined around each other completes the pattern, and the five labels all match up. This configuration is celebrated for its importance in the history of topology where it was observed (Weber and Seifert 1933) that it served as a symmetric model for Poincaré's *homology sphere* (Poincaré, 1904) which subsequently became known as his '*dodecahedral space*'. The vertices are themselves the centers of the tetrahedral cells of the dual regular polytope, the *600-cell*, and, while these vertex quaternions do not themselves form a group, the five inequivalent representatives within the dodecahedral space provide an obvious small set of five alternative orientations of an icosahedral grid, for example, and therefore an obvious candidate for a method of reducing grid-imprinting associated with the use of such a grid.

## 3. Small sets of rotated cubic grids

In Fig. 11 we show a color-coded map of the distances, in ten steps of 500 km, to the nearest edge of an inscribed cube, showing that a very large proportion of the global surface is necessarily fairly close to at least one edge. If we were tasked with arranging the locations of the center of a hurricane nest tracking the approximate path of the storm in its progression over several days, we would not be able to guarantee that, at some point in the duration of the storm, our nest would remain clear of the edges of the parent cubic grid if we had only the single orientation of the parent to choose from.

If we refer to the analysis of inequivalent rotations of the cube provided in section 2, we find that, by choosing the orientations identified by the centers of the octagonal faces of the fundamental region (whose Voronoi version is the projected truncated cube), we have a set of

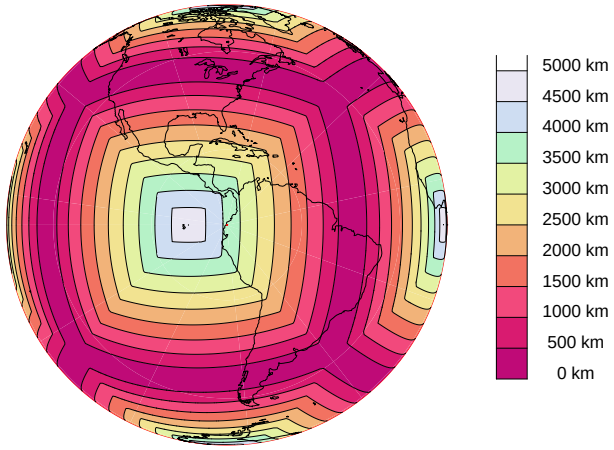


Figure 11. The distances, in steps of 500 km, along the surface of the globe to the nearest edge of the inscribed cube.

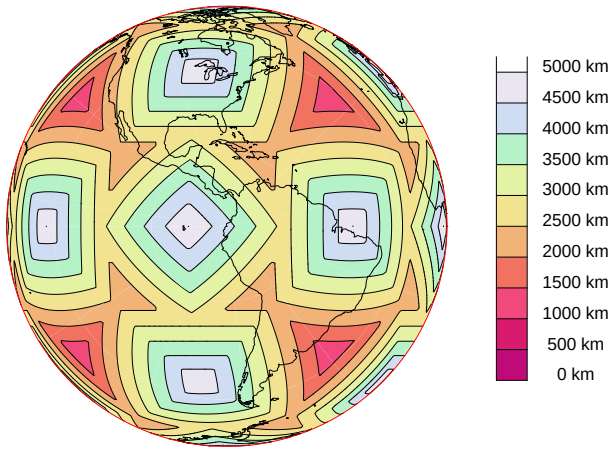


Figure 12. The largest radius, in steps of 500 km, a disk can have such there is a cube in the set of three whose edges do not intersect this disk.

three inequivalent orientations derived from the 'original' cube by rotating it 45° about one choice of its three principal Cartesian axes. If, in our nesting assignment, we have available this pool of parent grid orientations to choose from, then, as depicted in Fig. 12, our choice can ensure that, wherever on the globe our nest center happens to be, it is at least about 1000 km from the nearest edge of the parent cube.

Alternatively, if we construct our pool of parent grids from the six inequivalent vertices (A–F of Fig. 6), of the truncated cube fundamental region, the map of distances, shown in Fig. 13, is not an improvement. However, in this case, the 'bad' regions are themselves arranged in a pattern that matches the center of the faces of the original cube, so, breaking the 'democratic' symmetry of the set of six by including this seventh special member provides the edge-distance map, Fig. 14, which shows a dramatic improvement; now we are able to choose a parent cubic

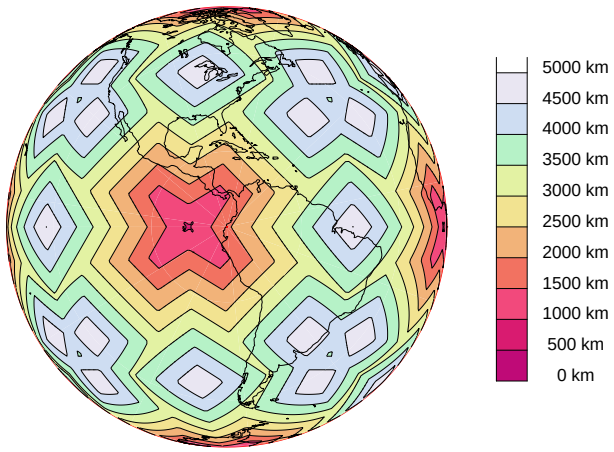


Figure 13. The largest radius, in steps of 500 km, a disk can have such there is a cube in the set of six whose edges do not intersect this disk.

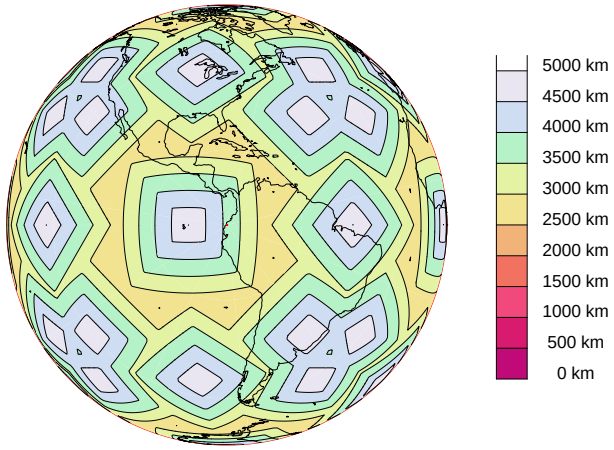


Figure 14. The largest radius, in steps of 500 km, a disk can have such there is a cube in the set of six-plus-one whose edges do not intersect this disk.

grid that ensures that a given geographical location is at least about 2500 km from the nearest edge. For the motion typical of a tropical storm, this would allow a period of at least a few days in which the nest could be maintained within the same parent before it would become necessary to restart the forecast with a new choice of parent from this pool of seven.

The icosahedral and octahedral groups share the tetrahedral subgroup in common. Five tetrahedra (four vertices) can be inscribed amongst the 20 vertices of the dodecahedron, which suggests the possibility that quintuples of cubes can be arranged to collectively possess the higher icosahedral symmetry. The simplest example occurs when the five tetrahedra inscribed in the dodecahedron carry with them the cubes in which they are also inscribed – that is, we can symmetrically inscribe five cubes in the dodecahedron such that each vertex of the dodecahedron is also a vertex of two of the cubes. If we designate one of these cubes to be the

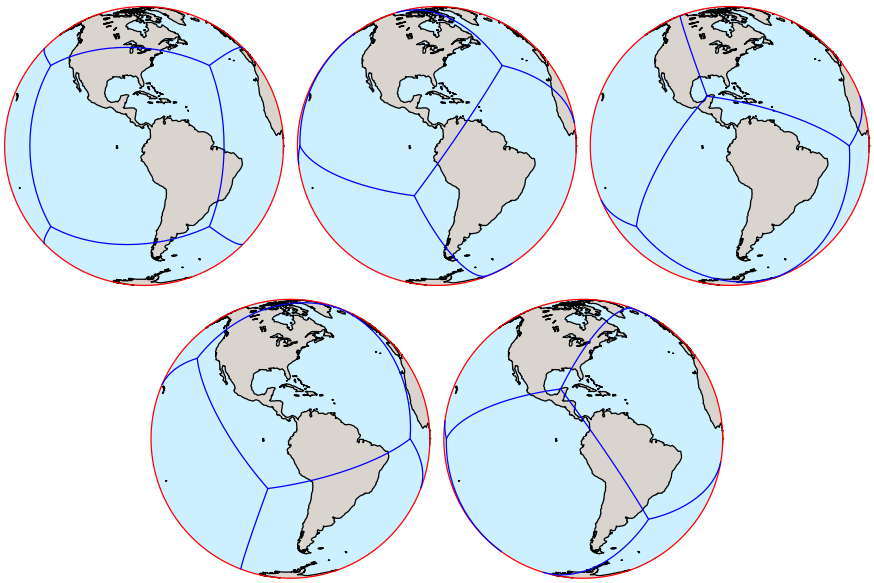

Figure 15. An example of a set of five cubes inscribed on the sphere that also correspond with their symmetrical inscription within a regular dodecahedron.

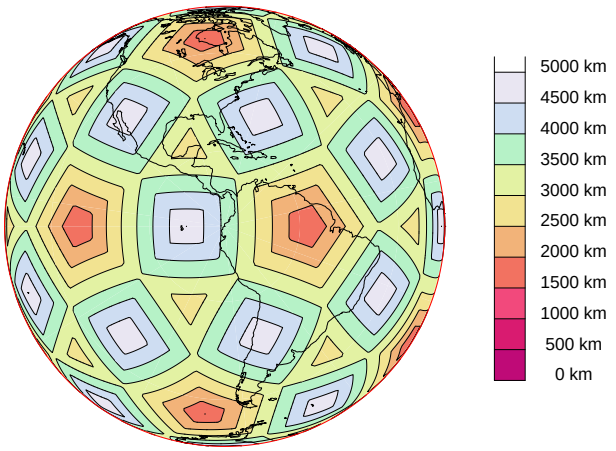


Figure 16. The largest radius, in steps of 500 km, a disk can have such there is a cube in the set of five whose edges do not intersect this disk.

'standard' (unrotated) version, we find that the other four cubic orientations are equivalent to equal rotations along the cube's long diagonal axes, in a tetrahedral arrangement. One such set of five cubes, as they appear inscribed on the globe, are shown in the five panels of Fig. 15. The edge distance map in this case is plotted in Fig. 16. The result is disappointing, but geometrically not surprising, since the 'bad' regions at the centers of each face of the dodecahedron are bound to be quite close to edges of all five inscribed cubes (the edges form a five-pointed star inscribed in the face in question). The edge distance we can guarantee for the

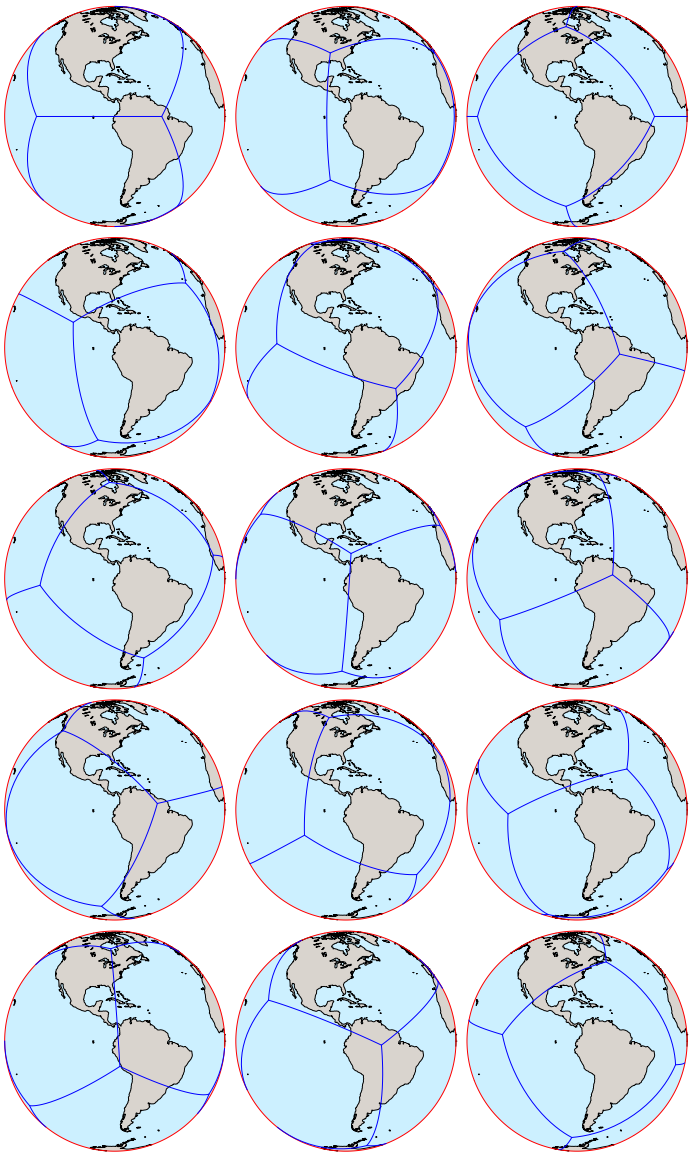

Figure 17. An example of a set of 15 cubes inscribed on the sphere that also correspond with their symmetrical inscription within a regular dodecahedron.

worst locations is only about 1500 km.

The other small set of cubes we can form by exploiting the icosahedral symmetry requires us to align the opposite edges of fifteen cubes with the opposite edges of the dodecahedron. Fig. 17 shows such a configuration of 15 cubes mapped to the globe. The edge distance map in this case is shown in Fig. 18 and shows that a cube from this pool of 15 can ensure a comfortable nearest edge distance of at least about 3250 km, and therefore a guarantee of several days of an uninterrupted forecast before it ever becomes necessary to regrid the

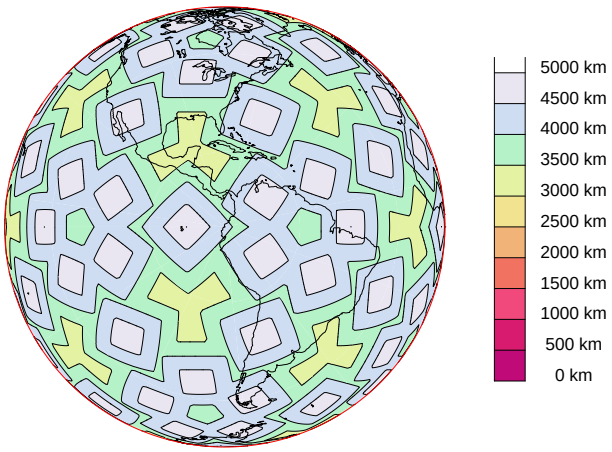


Figure 18. The largest radius, in steps of 500 km, a disk can have such there is a cube in the set of 15 whose edges do not intersect this disk.

parent and restart from a new orientation. Moreover, owing to the symmetry of the set, the accompanying relative orientations of one cube to another, apart from trivial relabeling of faces and their axes, amount to only four truly distinct relative orientations for which interpolation weights need be precomputed for these parent grids.

On the other hand, if the application is to avoid, as far as possible, the possibility that numerical 'resonance' artifacts impose a grid imprinting, this option provides a convenient set of 15 through which it is possible to cycle. In fact, by progressing through the cycle implied by concatenating, in order, the five rows of the displayed orientations of Fig. 17, we find that the 'distance' between each pair of consecutive orientations is as large as it is possible to make them from the options this set provides, and thus, a periodic regridding and restarting of an extended integration according to this cyclic schedule would provide a simple and sytematic way to minimize any possibility of spurious grid imprinting.

For ensembles, it may be desirable to be able to choose even larger sets of inequivalent orientations, which inevitably implies that useful ensemble members will no longer be 'democratically' symmetrical in the way that our sets of three, six, five and 15 are. The next section briefly discusses how we might address the problem of systematically choosing even larger sets of inequivalent orientations, not only of cubes, but of the other dihedral and icosahedral geometries, so as to fairly evenly cover the space of rotations to provide large diversified ensembles.

## 4. Larger sets

Should it be desirable to generate relatively large ensembles with their orientations distributed to evenly cover the space of inequivalent rotations, we can exploit the geometrical characterization of such rotations, not only for cubic grids, but also for those with dihedral or icosahedral symmetries. This section will present just a brief outline of systematic methods that can be applied to generate larger ensembles of each desired kind. For these larger sets, we only seek ensembles which, collectively, inherit the symmetries of one representative polyhedron of the chosen kind in its standard orientation.

First, we note that there is a characteristic convex polytope for each of the unit-quaternion sets that represent the various binary groups of the grids' symmetries, that is: the dicyclic group of order 16 for a square, or a square-prism, or an octagonal-dihedron grid; the binary-octahedral group of order 48 for a cubic grid; the binary-icosahedron group of order 120 for an icosahedral grid. In each case this polytope is formed as the convex-hull of the given unit quaternions that then constitute its set of vertices and, in each case, the cells of the resulting polytope are congruent polyhedra – the '*Delaunay*' tetrehedra. In each of the three cases this convex-hull polytope is the dual to the Voronoi polytope whose own polyhedral cells are the projections onto the tangent space at each of the unit-quaternion of the Voronoi domains we defined in section 2. The numbers of Delaunay tetrahedra for the square-dihedral, octahedral and icosahedral binary groups are respectively: 64; 288; 600. If we could systematically and symmetrically 'grid' these tetrahedra with an appropriate choice of a uniform grid of points, and find a mapping between the Delaunay polytope's 3D 'surface' and the $S_3$ of unit quaternions in such a way that the Jacobian of the mapping is uniform, then this same gridding of the Delaunay surface cells would also uniformly sample the space of rigid 3D rotations as represented by this double-cover of unit quaternions. Since we are interested only in the inequivalent rotations with respect to the underlying grid symmetry, the sufficient set of representative rotations are the quotients of the totals divided by the respective numbers of Voronoi cells and, in each case can found as the nonredundant quaternion images within, or on, a representative fundamental region (such as the Voronoi cell) implied by this uniform-Jacobian mapping from the Delaunay polytope back to the unit hypersphere.

One of the most elegant ways of constructing a uniform-Jacobian mapping is by way of a variational principle such as has been suggested in the slightly simpler context of gridding $S_2$ for global numerical models by the Eq. (20) of Rančić et al. (2017), which was itself a limiting case of a more general method proposed in Purser and Rančić (1998). Adapting this variational method to the present case, we imagine that a local Euclidean set of map coordinates, $\boldsymbol{x} = (x, y, z)^T$, covers the development into Euclidean 3-space of the Delaunay polytope, scaled such that the measure of the whole 'surface' in these coordinates equals that of the unit 3-sphere, i.e., $2\pi^2$. We seek the least distorted mapping between the $\boldsymbol{x}$ and the sphere $|\boldsymbol{q}| = 1$ subject to the Jacobian being unity:

$$G = q_0 \frac{\partial(q_1, q_2, q_3)}{\partial(x, y, z)} - q_1 \frac{\partial(q_0, q_2, q_3)}{\partial(x, y, z)} + q_2 \frac{\partial(q_0, q_1, q_3)}{\partial(x, y, z)} - q_3 \frac{\partial(q_0, q_1, q_2)}{\partial(x, y, z)} = 1. \tag{4.1}$$

Using Lagrange multiplier functions, $K$ and $\Lambda$, to guarantee the constraints of unit Jacobian and unit norm, the variational principle for this mapping looks like the extremization of:

$$\mathcal{L} = \frac{1}{2} \int\int\int \left[ \left| \frac{\partial \boldsymbol{q}}{\partial x} \right|^2 + \left| \frac{\partial \boldsymbol{q}}{\partial y} \right|^2 + \left| \frac{\partial \boldsymbol{q}}{\partial z} \right|^2 - 2K(G-1) + \Lambda(|\boldsymbol{q}|^2 - 1) \right] dx\, dy\, dz, \tag{4.2}$$

with respect to variations of $\boldsymbol{q}$, $K$ and $\Lambda$. This results in the Euler-Lagrange equations:

$$\frac{\partial^2 \boldsymbol{q}}{\partial x^2} + \frac{\partial^2 \boldsymbol{q}}{\partial y^2} + \frac{\partial^2 \boldsymbol{q}}{\partial z^2} = \boldsymbol{\nabla}_q K + \Lambda \boldsymbol{q} \tag{4.3a}$$

$$G = 1 \tag{4.3b}$$

$$|\boldsymbol{q}| = 1, \tag{4.3c}$$

where the operator, $\boldsymbol{\nabla}_q$, denotes the surface gradient with respect to the quaternion coordinates, $\boldsymbol{q}$.

In solving this problem numerically, one would obviously exploit the symmetry of the isometry group of rotations and reflections in the space of $\boldsymbol{q}$ to enormously reduce the size of the computational domain, and one could advantageously use a multigrid approach to find an accurate and efficient approximate solution. In the case of the dihedral and octahedral symmetries, the Voronoi decomposition of the surface of the Delaunay polytope does *not* map exactly to the Voronoi decomposition of unit quaternions on the 3-sphere because, as we mentioned in section 2, not all boundary surface elements of the fundamental region correspond to mirror planes of the isometry group, so the fundamental region is not the natural domain in which to solve our Euler-Lagrange equations. However, the faces of tetrahedral cells of the Delaunay polytope *do* lie in invariant planes of the isometry group. Therefore the correct solution is obtained by solving the Euler-Lagrange equations with Neumann boundary conditions in a central projection of a representative tetrahedron of the Delaunay polytope in each case of the polyhedral symmetries we have considered.

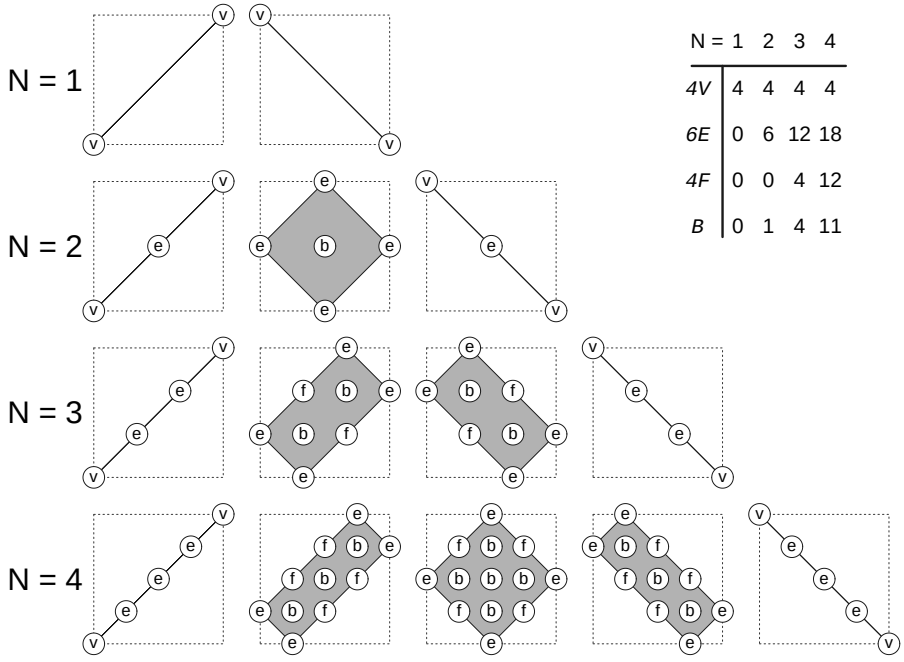


| N = | 1 | 2 | 3 | 4 |
|---|---|---|---|---|
| *4V* | 4 | 4 | 4 | 4 |
| *6E* | 0 | 6 | 12 | 18 |
| *4F* | 0 | 0 | 4 | 12 |
| *B* | 0 | 1 | 4 | 11 |

Figure 19. Slices in one family of principal planes of the simple cubic 'rc' lattice intersecting tetrahedrons (solid lines and shaded areas) inscribed in cubes (dotted outline) of different integer sizes, $N$, showing the locations of each type of intersection, marked 'v', 'e', 'f', 'b', corresponding respectively to the tetrahedron's geometrical element types: vertices, edges, faces or body-interior. The total tally for each $N$ and intersection type forms the table (inset) but the per-element tallies, the statistics $V$, $E$, $F$ are reduced by the factors 4, 6, and 4 that correspond to the numbers of vertices, edges and faces that the tetrahedron possesses.

There are four natural ways to grid a solid tetrahedron, based on cubic crystal lattices. Linearly mapping each tetrahedral region to a *regular* tetrahedron inscribed in a cube of sides $N$ lattice units, we then have the choice of gridding with: (i) a simple cubic lattice, registered with the vertices of the larger (size $N$) cube, which we call 'rc'; (ii) an off-set, or staggered,

simple cubic lattice, denoted 'oc'; (iii) the body-centered cubic lattice, here denoted 'bc'; (iv) the face-centered lattice, here denoted 'fc'. At each level of refinement, $N$, of the tetrahedral region we can easily find the number of lattice points per vertex, $V(N)$, per edge $E(N)$, per face $F(N)$ and per interior body $B(N)$, for each kind of lattice. Taking the registered (unstaggered) cubic lattice, rc, as an example, Fig. 19 shows, for the first four $N$, how the tally of the types, $V$, $E$, $F$ and $B$ intersections with the lattice relate to the geometry of slices through a tetrahedron inscribed in the cube with which the lattice is aligned. When a similar counting exercise is performed for the other lattices, the results are as tabulated for the first four $N$ in Table 1. For each lattice type, the $V$, $E$, $F$ and $B$ fit polynomials in $N$ of respective degrees, 0, 1, 2, 3, making the extrapolation of the table to higher $N$ very straightforward.

TABLE 1. Statistics, $V$, $E$, $F$, $B$, for each lattice type, rc; oc, bc and fc

| $N$ | $V_{rc}$ | $E_{rc}$ | $F_{rc}$ | $B_{rc}$ | $V_{oc}$ | $E_{oc}$ | $F_{oc}$ | $B_{oc}$ | $V_{bc}$ | $E_{bc}$ | $F_{bc}$ | $B_{bc}$ | $V_{fc}$ | $E_{fc}$ | $F_{fc}$ | $B_{fc}$ |
|---|---|---|---|---|---|---|---|---|---|---|---|---|---|---|---|---|
| 1 | 1 | 0 | 0 | 0 | 0 | 0 | 0 | 1 | 1 | 0 | 0 | 1 | 1 | 0 | 0 | 0 |
| 2 | 1 | 1 | 0 | 1 | 0 | 0 | 0 | 4 | 1 | 1 | 0 | 5 | 1 | 1 | 0 | 0 |
| 3 | 1 | 2 | 1 | 4 | 0 | 0 | 0 | 11 | 1 | 2 | 1 | 15 | 1 | 2 | 1 | 0 |
| 4 | 1 | 3 | 3 | 11 | 0 | 0 | 0 | 24 | 1 | 3 | 3 | 35 | 1 | 3 | 3 | 1 |

The gridding of the whole Delaunay quaternionic polytope by discretizing each of the constituent tetrahedra in this way gives rise to an implied total number of grid points that we can easily compute once we know this Delaunay polytope's total numbers of vertices, edges, faces and cell bodies, $O \times v$, $O \times e$, $O \times f$, $O \times b$, where $O$ is the order of the quaternionic group. Since we are only interested in the tally of these lattice points in a single fundamental region, it is the 'per-fundamental region' statistics that are of concern, and these are listed in Table 2 for the square dihedron, octahedral and icosahedral binary symmetry decompositions.

TABLE 2. Statistics, $v$, $e$, $f$, $b$, for each symmetry type

| Element type | Square dihedral | Octahedral | Icosahedral |
|---|---|---|---|
| $v$ | 1 | 1 | 1 |
| $e$ | 5 | 7 | 6 |
| $f$ | 8 | 12 | 10 |
| $b$ | 4 | 6 | 5 |

Now it requires only matrix multiplication to deduce, for each $N$, and for each symmetry type, how many quasi-uniformly distributed grid orientations this scheme provides for each of the lattice types. For $N \leq 4$ again, these are listed in Table 3 and can be extrapolated for larger $N$ by noting that the ensemble sizes are all cubics in $N$ in each column of the table.

The face-centered cubic (fc) and body-centered cubic (bc) lattices are both more efficient packing lattices than the simple cubic lattice (represented here by the rc and oc designations). While the fc lattice is more efficient than the bc in terms of packing, it has the relative disadvantage of having larger voids than the bc lattice. But these distinctions are of very minor significance, and we can expect all four methods of discretizing the fundamental domains of the rotation space implied by their intersections with the Delaunay tetrahedra to produce good representative samplings of the available domains.

TABLE 3. Sizes of ensembles possible with quasi-uniform distributions of rotations based on the four types of systematic gridding of the Delaunay simplexes and for refinement indices, $N \leq 4$, for the various symmetries.

| | Square dihedral | | | | Octahedral (cubic) | | | | Icosahedral | | | |
|---|---|---|---|---|---|---|---|---|---|---|---|---|
| $N$ | rc | oc | bc | fc | rc | oc | bc | fc | rc | oc | bc | fc |
| 1 | 1 | 4 | 5 | 1 | 1 | 6 | 7 | 1 | 1 | 5 | 6 | 1 |
| 2 | 10 | 16 | 26 | 6 | 14 | 24 | 38 | 8 | 12 | 20 | 32 | 7 |
| 3 | 35 | 44 | 79 | 19 | 51 | 66 | 117 | 27 | 43 | 55 | 98 | 23 |
| 4 | 84 | 96 | 180 | 44 | 124 | 144 | 268 | 64 | 104 | 120 | 224 | 54 |

## 5. Conclusions

Some systematic ways of 'randomizing' the orientations of polyhedral global grids have been presented exploiting the quaternionic geometry of rigid proper rotations and the associated symmetries. For the case of the cubic grid configuration, a related application is randomization of cubes for the purpose of providing a set of frameworks for the producing Hilbert space-filling curves. Advantageous small sets of rotated cubes can be found for three and for fifteen rotated forms in the democratic case where the members of the set are symmetrically equivalent to one another; there is also a very good nondemocratic set of seven rotated cubes where one member is distinguished from the rest.

For icosahedral symmetry, a set of five rotations of the cube preserves the symmetry among the members of the quintet (these correspond to the five distinctly-labeled vertices of Fig. 10) but adding a sixth member (corresponding to the center of the dodecahedron) would appear to improve the uniformity of the coverage of the rotation space.

When much larger ensembles are desired, we showed that a more systematic and generic approach is suggested by the regular gridding of the congruent tetrahedra of the quaternionic Delaunay polytope associated with each polyhedral symmetry, using one of four simple cubic crytallographic lattices to evenly discretize each tetrahedron to a resolution prescribed by an integer index, $N$. From this construction combined with a uniform-Jacobian mapping from the Delaunay polytope back to the 3-sphere, a single fundamental domain's-worth of the resulting lattice quaternions becomes equivalent to an ensemble of fairly evenly distributed inequivalent grid orientations, where the size of the ensemble is uniquely determined by the resolution index, $N$, and the choice of the crystallographic lattice employed in the gridding.

## Acknowledgments

The author is grateful to Dr. Tom Black for stimulating discussions on the nesting problem, and to Drs. Vladimir Krasnopolsky and David Parrish for their reviews.

## References

Bleck, R., and others 2015 A Vertically Flow-Following Icosahedral Grid Model for Medium-Range and Seasonal Prediction. Part I: Model Description. *Mon. Wea. Rev.,* **143,** 2386–2403.

| | | |
|---|---|---|
| Conway, J. H., and D. A. Smith | 2003 | *On Quaternions and Octonions; Their Geometry.* A. K. Peters, 176 pp. |
| Coxeter, H. S. M. | 1963 | *Regular Polytopes*, Dover, New York. 321 pp. |
| Coxeter, H. S. M. | 1970 | *Twisted Honeycombs* Conference Board of the Mathematical Sciences; Regional Conference Series in Mathematics, No. 4. American Mathematical Society, Providence, RI. 47 pp. |
| Gilmore, R. | 1974 | *Lie Groups, Lie Algebras, and some of their Applications* John Wiley and Sons, New York. |
| Lin, S.-J., and R. B. Rood | 1997 | An explicit flux-form semi-Lagrangian shallow water model on the sphere. *Quart. J. Roy. Meteor. Soc.,* **123,** 2477–2498. |
| Lyons, D. W. | 2003 | An elementary introduction to the Hopf fibration. *Math. Mag.,* **76,** 87–98. |
| Poincaré, H. | 1904 | Cinqueiême complément à ánalysis situs. *Rend. Circ. Mat. Palermo,* **18,** 45–110. |
| Purser, R. J., and Rančić, M. | 1997 | Conformal octagon: an attractive framework for global models offering quasi-uniform regional enhancement of resolution. *Meteor. Atmos. Phys.,* **62,** 32–48. |
| Purser, R. J., and Rančić, M. | 1998 | Smooth quasi-homogeneous gridding of the sphere. *Quart. J. Roy. Meteor. Soc.,* **124,** 637–647. |
| Purser, R. J., M. de Pondeca, and S.-Y. Park | 2009 | Construction of a Hilbert curve on the sphere with an isometric parametrization of area. NOAA/NCEP Office Note 460. |
| Purser, R. J., and M. Tong | 2017 | A minor modification of the gnomonic cubed-sphere grid that offers advantages in the context of implementing moving hurricane nests. NOAA/NCEP Office Note 486. |
| Putman, W. M., and S.-J. Lin | 2007 | Finite-volume transport on various cubed-sphere grids. *J. Comput. Phys.,* **227,** 55–78. |
| Weber, C., and H. Seifert | 1933 | Die beiden Dodekaederräume. *Math. Z.,* **37,** 237–253. |